Available online at www.sciencedirect.com

SCIENCE DIRECT

Diamond & Related Materials 14 (2005) 928–933

DIAMOND AND RELATED MATERIALS

www.elsevier.com/locate/diamond

Growth and characterisation of polymeric amorphous carbon and carbon nitride films from propane

G. Fanchini[a,*], P. Mandracci[a], A. Tagliaferro[a], S.E. Rodil[b], A. Vomiero[c,d], G. Della Mea[c,e]

[a]*Dipartimento di Fisica, Politecnico di Torino, Corso Duca degli Abruzzi 24, I-10129 Torino, Italy*
[b]*Instituto de Investigaciones en Materiales, UNAM, Coyoacan, México D. F, Mexico*
[c]*Laboratori Nazionali di Legnaro, Istituto Nazionale di Fisica Nucleare, Padova, Italy*
[d]*Dipartimento di Fisica, Università di Padova, Padova, Italy*
[e]*Dipartimento di Ingegneria, Università di Trento, Trento, Italy*

Available online 8 April 2005

Abstract

In this work, we report about the deposition of a-C(N):H films by electron–cyclotron–resonance using propane as a carbon precursor. The films generally present high H contents (up to 61 at.%) and large optical gaps. The maximum N content we obtained is 13 at.%. In nitrogenated films, we observed a strong decrease of the stretching intensity of the infrared spectra of the hydrocarbon (CH_n) vibrations, even at very low nitrogen content, the H content being still comparable to that of pure a-C:H. The various phenomena that can lead to such an effect are discussed: (i) different type of hydrogen bonding (CH_n and NH_n) in presence and in absence of nitrogenation; (ii) weakening of the cross-section of the CH_n groups in presence of nitrogen; (iii) large presence of non-bonded hydrogen meaning, with this, either the presence of molecular H2 or unbounded hydrogen. In addition, the residual amount of IR absorption due to C–H vibrations shows that, in a-CN:H, C–H bonded and non-bonded hydrogen does coexist.

Keywords: Diamond-like carbon; Carbon nitride; Plasma CVD; Bonding configurations

1. Introduction

Carbon nitrides are interesting materials both for fundamental and application purposes. The nitrogen bonding regime in such materials is a strongly debated issue [1–5]. Perspective applications of carbon nitride films range from hard disk protections [6] to electroluminescent devices [7] to biomedical coatings [8] and sensors. Carbon nitrides were originally studied in light of the preparation of super-hard, crystalline, C_3N_4 phases [1]. However, most of the applications expected nowadays do not rely neither on hardness nor on crystallinity. Since hydrogen has been generally foreseen as an obstacle leaning on the formation of C_3N_4 crystallites [1], hydrogenated carbon nitrides (a-CN:H) with high hydrogen contents were seldom studied [9,10].

If the nature of nitrogen bonding in amorphous carbon nitrides is still debated, also the mechanisms governing the hydrogen bonding are not yet clear. In hydrogenated amorphous carbon (a-C:H), though an early report [11] suggested that in extreme cases the fraction of non-bonded hydrogen could reach 50%, it is now generally accepted that the most part of hydrogen is bonded in hydrocarbon (CH_n) groups, preferentially with sp^3 carbon sites, and the fraction of unbounded hydrogen is low [12–14]. This is in contrast with what happens in hydrogenated amorphous silicon (a-Si:H) [15] where it is commonly accepted that a relevant H fraction is non-bonded. The difference has been roughly justified by observing that the Si–H bonds are weaker than the C–H bonds [6]. Dealing with a-CN:H, there is a number of works [3,10,16–18] reporting, upon nitrogen addition, a strong weakening of the infrared vibrations at 2800–3100 cm^{-1}, related to the CH_n groups: the explanations, however, are not exhaustive. It has been suggested [3,10,16,17] that, increasing the N content, amino (NH_n) groups gradually

* Corresponding author. Fax: +39 011 5647399.
E-mail address: giovanni.fanchini@polito.it (G. Fanchini).

0925-9635/$ - see front matter © 2005 Elsevier B.V. All rights reserved.
doi:10.1016/j.diamond.2005.01.030

replaces the CH_n groups. However, no definite evidence of the NH_n groups was found. In the infrared spectra, amino groups would provide narrow stretching peaks at ~3400 cm^{-1} and, also, sharp bending and rocking-wagging peaks at ~1600 and 1210 cm^{-1} [19]. Such peaks have never been detected safely. In contrast, the very broad absorption band that is often observed at ~3400 cm^{-1} in the infrared spectra of low-density amorphous carbon nitrides, either deliberately hydrogenated or not, was shown to not shift upon isotopic replacement of hydrogen with deuterium [4,20]. Then, such a broad band, formerly assigned to NH_n, is now generally assigned [1,4,5,18] to hydroxyl (OH) inclusions absorbed in the pores of the material after its exposure to atmospheric water vapour. Furthermore, this explanation easily accounts for the broad band width in terms of hydrogen bonds, OH···OH. However, due to the generally low oxygen contents, only little fraction of hydrogen is bonded in such way. Thus, comparing a-C:H and a-CN:H, the presence of H bonded as OH cannot account for the strong reduction, at still comparable H contents, of the infrared features due to CH_n groups.

Even dealing with non-bonded hydrogen, the

In this paper, we will report on a-C(N):H films with high H content (>60 at.%), prepared by electron–cyclotron–resonance (ECR) from propane. To our knowledge, the H contents of our films (>50 at.%) are the highest ever reported in presence of nitrogen. The present study is somewhat complementary to a similar work [18] we performed on graphite-like a-CN:H and a-C:H samples with low H content (below 25 at.%), prepared by reactive sputtering. Also in that case, we observed an important drop of the IR absorption of the CH_n groups after N addition. We will then focus on the role played by hydrogen, accomplishing the characterisation directly showing hydrogen (infrared spectroscopy and compositional analysis by nuclear techniques) with X-ray photoemission spectroscopy (XPS) data.

2. Experimental

The films were grown in a 2.45 GHz ECR system described elsewhere [20]. For the preparation of a-C:H, a propane flow has been injected as a reactive gas in the gas inlet ring while argon (Ar) or hydrogen (H_2) was excited in the upstream ECR region and used as excitation gases. a-CN:H films were grown using either hydrogen–nitrogen mixtures (N_2+3H_2) or pure nitrogen in the plasma stream at microwave powers, total pressures and reactive to carrier gases flow ratios similar to those used to grow the a-C:H films. In all cases, the carrier to reactive gas flow ratio was 5:1.

Different substrates were used: pyrex glass, doped and undoped Si(111) wafers, stainless steel. During the depositions, the substrate holder was kept at a fixed temperature of 60 °C through a regulating loop, in order to avoid changes in the growth conditions caused by progressive self-heating. The deposition times were kept fixed at 1 h for a-C:H and 1 h and 30 min for a-CN:H, which provided, due to different deposition rates, films of different thicknesses (see Table 1).

All the samples were analysed by means of nuclear techniques. Nuclear reaction analysis (NRA) was used to detect the relative carbon, nitrogen and oxygen content. An $^2H^+$ beam at 1.0 MeV was applied, and the following reactions were considered: $^{12}C(d,p_0)^{13}C$, $^{14}N(d,p_{1+2})^{15}N$, $^{14}N(d,\alpha_1)^{12}C$, $^{16}O(d,p_1)^{14}N$. All the spectra were processed using the RUMP code. Rutherford back-scattering (RBS) analysis by the means of a 2.2 MeV $^4He^+$ beam at a scattering angle θ=160° was used to benchmark the results of NRA.

The hydrogen content was estimated by means of elastic recoil detection (ERD) analysis. A 2.2 MeV $^4He^+$ beam was applied, at a forward scattering angle θ=150° and a 75° tilt angle of the sample axis with respect to the beam direction. A 10 μm mylar foil was used as stopping medium for the forward scattering of the primary beam. Due to H desorption during spectra acquisition as a consequence of ion bombardment, the ERD spectra were processed according to Ref. [21] in order to extract information on the hydrogen areal density. The hydrogen in-depth distribution was calculated by applying the proton elastic recoil cross-section reported by Kim et al. [22].

The XPS data were recorded on a Multilab ESCA 2000 VG Microtech instrument, using the Al K_α radiation

Table 1
Relevant data of the samples: preparation conditions (chamber pressure, microwave power, used carrier gases), composition, total intensity of the hydrocarbon stretching peaks (N_{CHn}), Tauc optical gaps (E_g), static refractive indexes (n_0) and thicknesses (d)

Sample (type)	p (mTorr)	Pow (W)	Carrier gas	N (at.%)	O (at.%)	H (at.%)	N_{CHn} (cm^{-1})	E_g (eV)	n_0	d (nm)
#133 (a-C:H)	20	700	H_2	–	2.2	61.3	370	3.79	1.48	150
#134 (a-C:H)	10	700	H_2	–	1.6	55.3	373	3.55	1.49	130
#135 (a-C:H)	5	700	H_2	–	1.8	49.3	337	3.42	1.56	120
#136 (a-C:H)	3	700	Ar	–	2.7	46.1	192	3.18	1.67	130
#137 (a-C:H)	3	350	Ar	–	1.7	54.4	237	3.45	1.54	100
#138 (a-C:N:H)	3	700	$3H_2+N_2$	6.4	5.9	46.9	35	2.97	1.68	30
#139 (a-C:N:H)	5	700	$3H_2+N_2$	2.9	3.2	51.8	75	3.35	1.66	80
#140 (a-C:N:H)	10	700	$3H_2+N_2$	5.0	3.5	49.6	51	3.35	1.74	30
#141 (a-C:N:H)	20	700	$3H_2+N_2$	<1	8.3	50.0	81	3.56	1.62	20
#142 (a-C:N:H)	10	350	N_2	13.1	7.9	34.8	31	2.65	1.95	120

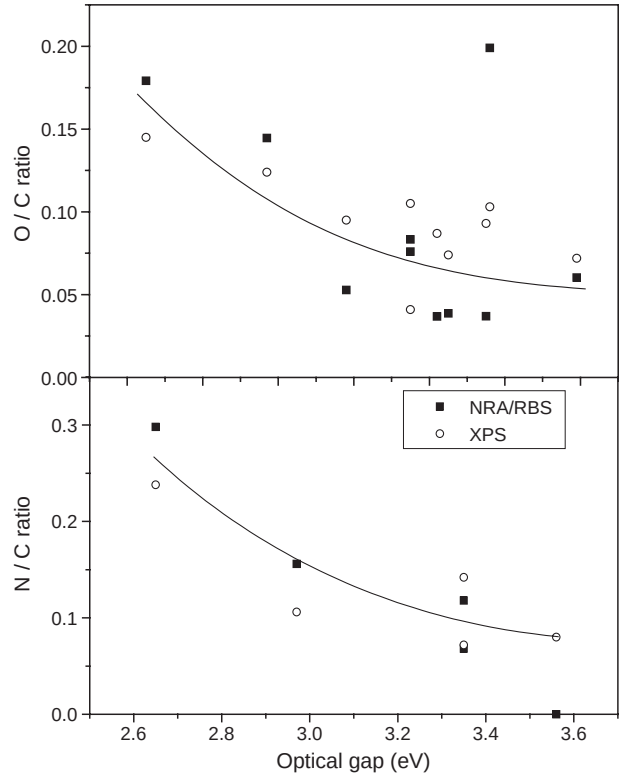

Fig. 1. Comparison of the N/C and O/C stoichiometric ratios of our samples, as estimated by NRA/RBS and XPS measurements. Sample #141 is at odd since, although N could not be detected by nuclear techniques, it was shown to be nitrogenated by XPS measurements performed on the whole cross-section of the sample as detailed on Section 2.

(1486.6 eV) as X-ray source and an Ar^+ ion gun for the in-situ treatment of the samples: on selected samples, the XPS measurements were carried out not only on the as-grown film, but also after sessions of 20s Ar^+ erosion of the sample at an Ar^+ current of 1.5 μA and 3 kV acceleration potential in order to obtain a cross-sectional XPS composition.

The FTIR spectra were collected on a Perkin-Elmer FTIR 2000 spectrometer. Once the film thicknesses were determined (Tencor profilometer), the static refractive index (n_0) was extracted from a simulation of the interference fringes which modulate the IR backgrounds. The FTIR spectra were normalised by the film thicknesses and fitted with standard routines assuming a Gaussian peak for each vibrational contribution in the stretching and bending frequency regions of the CH_n groups (respectively 2700–3200 cm^{-1} and 1300–1500 cm^{-1}). Raman measurements were recorded on a Renishaw Ramanscope system using the 514.5 nm line of an Ar^+ laser. However, the Raman signals of the samples were not detectable since, as usual in polymer-like a-C(N):H, they are completely overwhelmed by a strong photoluminescence background. Conventional optical (Varian Cary spectrometer) and photothermal deflection (PDS) measurements were used to determine the Tauc optical gaps.

3. Results and discussion

3.1. Sample composition

Fig. 1 compares the N and O contents of our a-CN:H films detected by nuclear and XPS methods. We find a fairly good agreement between such different techniques. This happens although the two kinds of measurements bear a very different meaning: the XPS data are only surface-sensitive and can easily separate bonded and unbounded elements, while the RBS and NRA data monitor the whole bulk of the film, irrespectively on its bonded or bonding nature.

Fig. 2a reports the hydrogen contents of our films, either nitrogenated or not, as a function of the Tauc gap. Our data are compared to other literature data, from samples grown either by ECR and other methods. The nitrogen content of our samples, measured by RBS and NRA, is always below 15 at.% (Fig. 2b). Apparently, Fig. 2a can be fully understood in terms of the structural models of nitrogen-free a-C:H. Indeed, higher H contents provide either lower amounts of distortions [23] or smaller clusters of sp^2 carbon sites [24] and, according to the "cluster model" of a-C:H, both effects involve larger energy spacing between the π and π* electronic states. However, the data of Fig. 2a are very scattered, especially at low gaps. Moreover, Fig. 2b

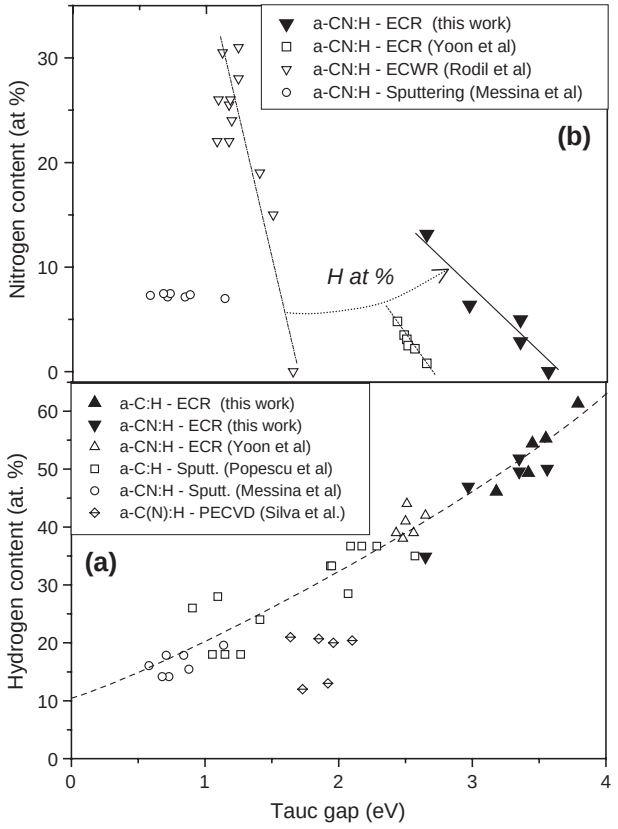

Fig. 2. (a) Hydrogen content and (b) nitrogen content of our samples compared to literature samples with lower optical gaps. Data from Refs. [3,9,13,17,18].

shows that the gap is also affected by the nitrogen contents and it changes in different ways in samples grown by different techniques. Thus, also the role of other effects, such as, for instance, the role of lone pair electrons of nitrogen [25] could be important in controlling the gap. From Fig. 2a, we may conclude that, especially at low nitrogen incorporation, the hydrogen content importantly affects the optical properties since, irrespectively of nitrogen, samples with more H always involve higher gaps.

3.2. Hydrogen

Except for the samples #138, #140 and #141, which are too thin to be modelled, the simulation of the ERD spectra was able to determine the profile of the hydrogen content. In the a-C:H samples, the cross-sectional variations of the H content are below the relative uncertainty of the hydrogen detection by ERD. Only in sample #136, the less hydrogenated one, the ERD spectrum highlights an inhomogeneous H in-depth profile (Fig. 3c), with H content at the surface 25% higher than at the interface with the substrate.

Dealing with the a-CN:H samples, an interesting cross-sectional variation of the H content is found on sample #142, having the highest N content and, again, being the less hydrogenated one (Fig. 3d): here, we can observe a maximum relative variation of 55% of the H concentration on the profile. Fig. 3d also shows the XPS cross-sectional analysis of the film, performed by a sequence of in situ erosions of the sample for 20 s, each one of them followed by an XPS measurement. We note that the nitrogen content diminishes from the surface to the bulk, while the H content has a maximum at approx. 30% of the cross-section.

We can also observe that in our samples the total H content does not importantly decrease upon little nitrogen addition. It always remains above 45 at.% for N incorporation below a threshold of approx. ~10 at.%. This agrees with the data of Yoon et al. [9], showing H contents of ~40 at.%, with changes within the uncertainty of the measurements, on weakly nitrogenated ECR samples grown from methane. Also in the samples grown by PECVD, there is only little change in hydrogen content at N incorporation below ~10–12 at.%, as reported in Refs. [3,16].

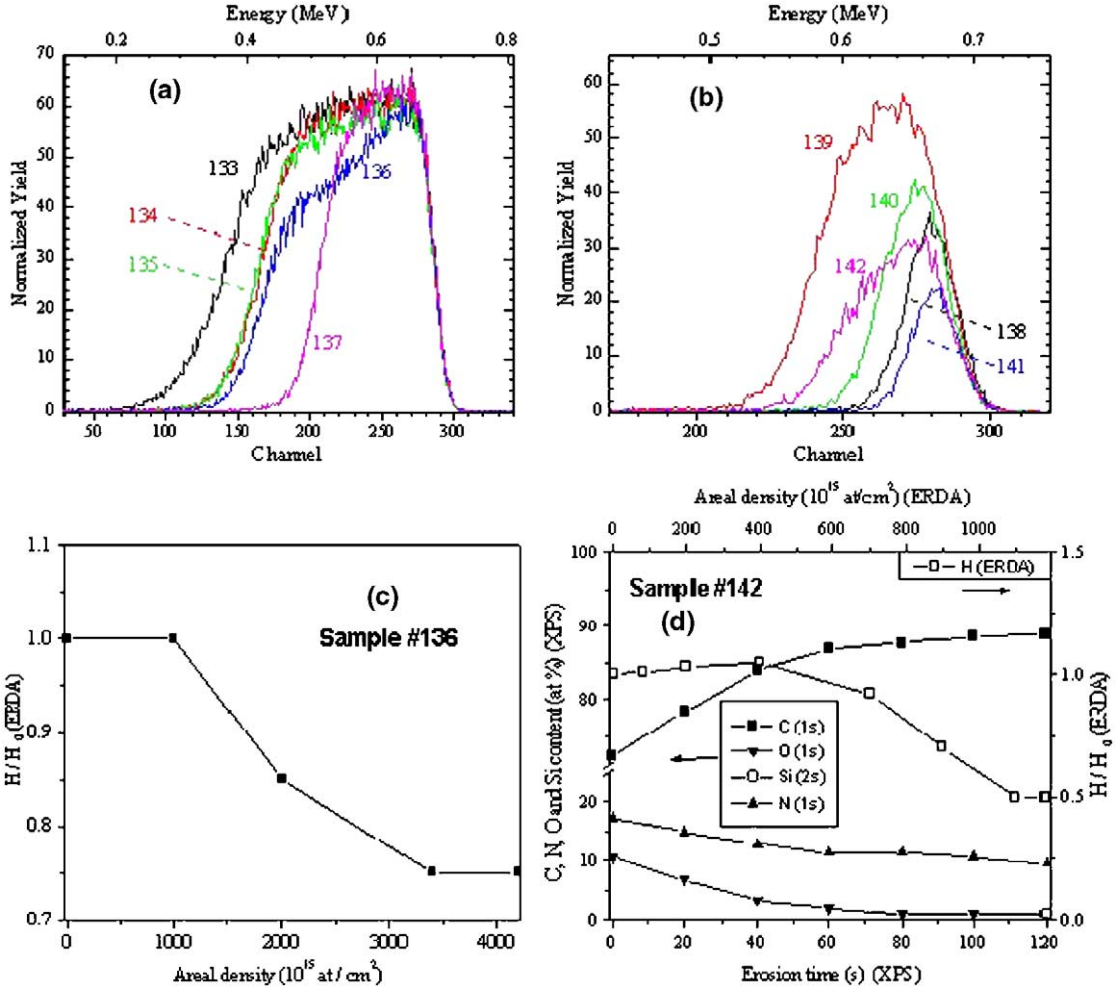

Fig. 3. ERD spectra of our samples (panel a: a-C:H samples and panel b: a-CN:H samples). The cross-sectional ERD profiles of the two samples having the highest cross-sectional inhomogeneities are shown in panels c and d. In panel d, the C, N and O profiles obtained by the XPS data are also shown.

Comparing a-C:H and a-CN:H, we could therefore expect that, in absence of changes in hydrogen bonding regime and electronic structure, the H-related features in the infrared spectra would be reasonably similar in shape, and scaled in intensity with the H concentration. Fig. 4 and Table 1, however, show that this is not the case. From sample #134 (a-C:H) to sample #140 (a-CN:H), the only difference in growth conditions is the replacement of 25% of the H_2 flux with an equal N_2 flux. However, the total stretching and bending intensity of the CH_n groups reduces by a factor 7. From sample #137 (a-C:H) to the sample #142 (a-CN:H), the Ar flux is replaced with an equal flux of N_2: the total CH_n stretching intensity diminishes by a factor 8. According to the peak positions of Ref. [6], the Gaussian fit of the CH_n features shows that there is no important change in the vibrations types of a-C:H and a-CN:H but, simply, an important decrease in intensity. In the next subsections, we will discuss the reasons they can lead to such an effect.

3.2.1. Conversion to other hydrogen bonding regimes

As already mentioned in the Introduction, the lowering in intensity of the CH_n vibrational peaks at 2800–3100 cm^{-1} after N addition was often attributed to a conversion to other bonding regimes, namely the appearance of NH_n groups. The attribution of the broad absorption at ~3300 cm^{-1} to OH vibrations instead of NH_n was not sufficient to rule out such a conversion since the N–H bonds are weakly polar and, hence, they might involve a weak infrared cross-section. However, dealing with samples #138–#140 (nitrogen contents of 6.4 at.%, 2.9 at.% and 5.0 at.%, respectively, detected by NRA) we note that the maximum H contents as NH_2 we can hypothesise are 12.8 at.%, 5.8 at.% and 10 at.%, respectively, and they could justify only a very little fraction of the drop of the IR peaks at 2700–3100 cm^{-1}.

Hence, in the present work, through the preparation and the analysis of highly hydrogenated samples, we are able to definitely rule out the present hypotheses.

3.2.2. Modifications of the infrared cross-sections by local fields

Actually, dealing with the intensities of the IR peaks as in Section 3.2.1, we have also to consider that the absorption $\alpha_i(\omega)$ of an infrared-active mode does not only depend on the concentration N_i of the oscillating group but also, on its infrared cross-section C_i:

$$N_i = \frac{1}{C_i}\int \frac{\alpha_i(\omega)d\omega}{\omega} \propto \frac{1}{e^{*2}_i \cdot f(n_0)}\int \frac{\alpha_i(\omega)d\omega}{\omega} \qquad (1)$$

C_i mainly depends on two factors [26]:

(i) The dynamic effective charge e^*_{0i} which is a property of the considered i-mode. Values of e^*_{0i} for the hydrocarbon modes can be found on Ref. [26].
(ii) The local field correction f affecting the effective charge due to its location on a specific environment with a given refractive index n_0. Different models can be drawn in order to estimate $f(n_0)$ [27]. However, if the electronic transitions occur far from the infrared range, f always increases at increasing n_0 and, hence, at decreasing optical gap.

n_0 weakly increases upon nitrogenation (see Table 1). Hence, also the infrared cross-section would weakly increase

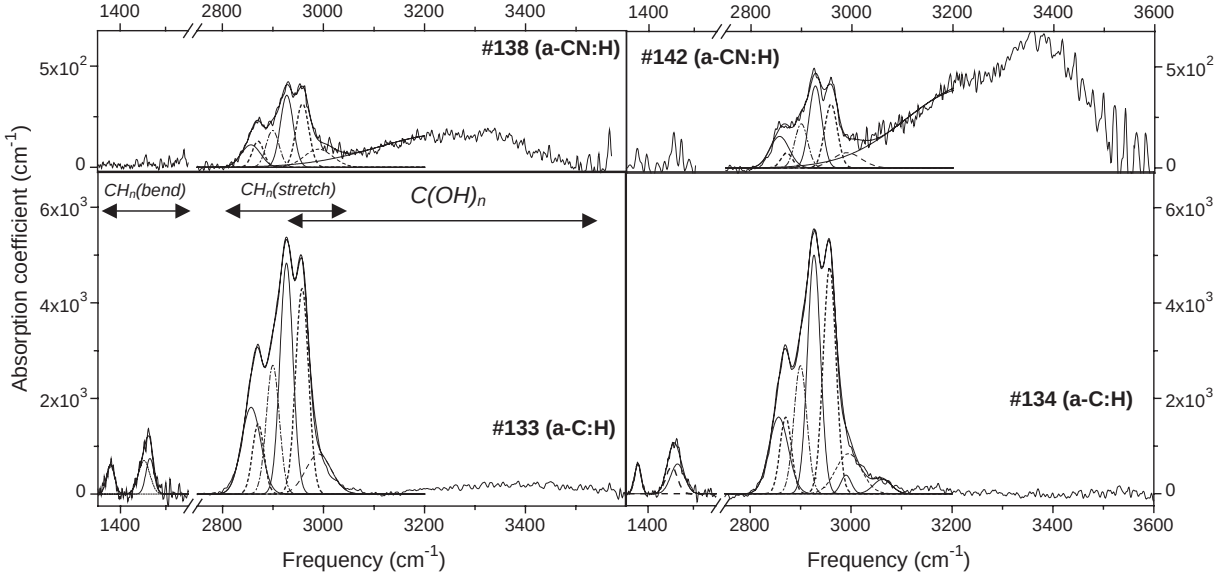

Fig. 4. Most prominent IR features of the most nitrogenated a-CN:H samples (upper panels) and the most hydrogenated a-C:H samples (lower panel). The following Gaussian peaks were used to deconvolute the CH_n features [6,26]: Csp^3H (2895 cm^{-1}); Csp^3H_2 (symmetric stretching: 2825 cm^{-1}, asymmetric stretching: 2920 cm^{-1}, bending: 1465 cm^{-1}); Csp^3H_3 (symmetric stretching: 2860 cm^{-1}, asymmetric stretching: 2955 cm^{-1}, symmetric bending: 1375 cm^{-1}, asymmetric bending: 1455 cm^{-1}); Csp^2H (stretching at approx. 3000 cm^{-1}, bending below the detectable intensity level). In all a-CN:H samples, the stretching intensity dramatically lowers, as in Table 1, and the bending peaks are almost undetectable.

while, in order to justify the important drop of $\alpha_i(\omega)$ at not too different hydrogen concentrations, we would have needed an important decrease of C_i. Also the present hypothesis is then untenable.

3.2.3. Non-bonded configurations

We may then admit that little nitrogen amounts in the carbon network can involve large amounts of non-bonded hydrogen. It is worth noting that, in the present paper, the term "non-bonded" may refer either to unbounded hydrogen, like in a-Si:H [15] or to adsorbed H_2 molecules, as in other materials. At least at a first sight, the hypothesis of H_2 molecules would be in contrast with the finding that the optical gap, both in a-C:H and a-CN:H, correlates with the H content (Fig. 2a). Indeed, the optical gap in a-C:H is mainly determined [24] by the concentration of a typical sp^2 carbon cluster. As well known [28,29], this implies that the sp^2 carbon clustering is controlled by the presence of hydrogen linked to the network (either in a stably bonded configuration or in a metastable bonding regime [15] or in other possible situations), since this is a necessary condition to promote the sp^3 carbon sites separating the sp^2 clusters.

However, since amorphous carbon nitrides are somewhat different to amorphous carbons, other effects may come into play and further work is required to achieve a more detailed knowledge to the coexistence, in a-CN:H, of non-bonded hydrogen and hydrogen bonded as CH_n groups.

4. Conclusions

In conclusion, our study has shown that in polymer-a-C:H, one effect of even low N addition (5–15%) is in lowering of one order of magnitude the intensity of the IR absorption related to CH_n groups. The phenomenon occurs at hydrogen contents comparable to that of nitrogen-free carbon nitrides grown under similar conditions.

We have not found clear signatures of the presence of amino (NH_n) groups. However, even assuming that the whole amount of N in the films would be bonded as NH_2, the low N content will rule out the possibility that the decrease in concentration of the CH_n groups is due to a compensating increase of the NH_n groups concentration.

Also, the hypothesis that the drop of the IR absorption of the CH_n groups is due to an important lowering in the IR cross-section is not likely. It should be accompanied by a dramatic decrease of the refractive index or, equivalently, a gap increase after N addition. These optical parameters slightly change in the opposite way.

Therefore, we must hypothesise that, upon little nitrogen addition, the hydrogen incorporation largely occurs into non-bonded forms (metastable bonding and/or H_2 molecules) in coexistence with a residual amount of C–H bonds.

Acknowledgements

We are grateful to L. Huerta for the XPS measurements. This work was partially supported by a MAE/SRE-CONACYT Italy/Mexico collaborative project.

References

[1] S. Muhl, J.M. Mendez, Diamond Relat. Mater. 8 (1999) 1809.
[2] J.H. Kaufman, S. Metin, D.D. Saperstein, Phys. Rev. B39 (1989) 13053.
[3] S.R.P. Silva, J. Robertson, G.A.J. Amaratunga, et al., J. Appl. Phys. 81 (1997) 2626.
[4] S.E. Rodil, S. Muhl, Diamond Relat. Mater. 13 (2004) 1521.
[5] G. Fanchini, A. Tagliaferro, S.C. Ray, Diamond Relat. Mater. 12 (2003) 208.
[6] J. Robertson, Mater. Sci. Eng. R37 (2002) 129.
[7] M. Zhang, Y. Nakayama, M. Kume, Solid State Commun. 110 (1999) 679.
[8] S.E. Rodil, R. Olivares, H. Arzate, S. Muhl, Diamond Relat. Mater. 12 (2002) 931.
[9] S.F. Yoon, Rusli, J. Ahn, et al., Thin Solid Films 340 (1999) 62.
[10] M. Camero, R. Gago, C. Gomez-Alexaindre, J.M. Albella, Diamond Relat. Mater. 12 (2003) 632.
[11] A. Grill, V. Patel, Appl. Phys. Lett. 60 (1992) 2089.
[12] C. Donnet, J. Fontaine, F. Lefèbvre, A. Grill, V. Patel, C. Jahnes, J. Appl. Phys. 85 (1999) 3264.
[13] B. Popescu, C. Verney, E.A. Davis, V. Paret, A. Brunet-Bruneau, J. Non-Cryst. Solids 266–269 (2000) 778.
[14] J. Ristein, S.T. Stief, L. Ley, W. Beyer, J. Appl. Phys. 84 (1998) 3836.
[15] R.A. Street, Hydrogenated Amorphous Silicon, Cambridge University, 1985.
[16] P. Wood, T. Wydeven, O. Tsuji, Thin Solid Films 258 (1995) 151.
[17] S.E. Rodil, A.C. Ferrari, J. Robertson, W.I. Milne, J. Appl. Phys. 89 (2001) 5425.
[18] G. Messina, S. Santangelo, G. Fanchini, et al., Diamond Relat. Mater. 11 (2002) 1166.
[19] G. Herzberg, Molecular Spectra and Molecular Structure, vol. II, Van Nostrand, New York, 1945.
[20] J.P. Conde, V. Chu, M.F. daSilva, et al., J. Appl. Phys. 85 (1999) 3327;
P. Mandracci, PhD thesis, Politecnico di Torino, 2001.
[21] A. Monelli, F. Corni, R. Tonini, C. Ferrari, G. Ottaviani, J. Appl. Phys. 80 (1996) 109.
[22] S.K. Kim, H.D. Choi, Nucl. Instrum. Methods B174 (2001) 33.
[23] J. Robertson, Diamond Relat. Mater. 4 (1995) 297.
[24] J. Robertson, E.P. O'Reilly, Phys. Rev. B35 (1987) 2946.
[25] G. Fanchini, A. Tagliaferro, N.M.J. Conway, C. Godet, Phys. Rev. B66 (2002) 195415.
[26] T. Heitz, B. Drévillon, C. Godet, J.E. Bourée, Phys. Rev. B58 (1998) 13957.
[27] M.H. Brodsky, M. Cardona, J.J. Cuomo, Phys. Rev. B16 (1977) 3556.
[28] J. Jansen, J.C. Angus, J. Vac. Sci. Technol., A, Vac. Surf. Films 6 (1988) 1778.
[29] J. Robertson, Phys. Rev. Lett. 68 (1992) 220.